



Feature-preserving, mesh-free empirical mode decomposition for point clouds and its applications [☆]



Xiaochao Wang ^{a,c}, Jianping Hu ^{b,c,*}, Lixin Guo ^c, Dongbo Zhang ^c, Hong Qin ^d,
Aimin Hao ^c

^a School of Science, Tianjin Polytechnic University, Tianjin 300387, China

^b College of Sciences, Northeast Electric Power University, Jilin 132012, China

^c State Key Laboratory of Virtual Reality Technology and Systems, Beihang University, Beijing 100191, China

^d Department of Computer Science, Stony Brook University, Stony Brook, NY 11794-4400, USA

ARTICLE INFO

Article history:

Received 27 September 2016

Received in revised form 25 May 2017

Accepted 22 November 2017

Available online 5 December 2017

Keywords:

Empirical mode decomposition

Point clouds

Feature-preserving analysis and processing

Multi-scale decomposition

Structure measurement

ABSTRACT

Point clouds have been extensively employed to represent 3D shapes with the increasing availability of various data acquisition devices/technologies. As a result, more novel techniques are urgently needed for point clouds' analysis and processing. To date, empirical mode decomposition (EMD) has become a powerful and effective analytical tool for non-stationary, non-linear signals, and has been widely applied to time series processing. Despite the fact that EMD has exhibited its potential in 3D geometry processing, extending the existing techniques of EMD to operate directly on point clouds remains to be extremely challenging. This is primarily because of imperfect point clouds, as well as their absence of topological information. In this paper, we develop a multi-scale mesh-free EMD algorithm for point clouds and their analysis and processing. The multi-scale mesh-free EMD is achieved by iteratively extracting the detail level from the input signal and leaving the overall shape in residue. Furthermore, in order to preserve sharp features during point-based EMD analysis/processing, we devise an anisotropic structure measurement assisted envelope computation scheme. The structure measurement is computed by the eigenvalue decomposition of voting tensor, which could faithfully characterize the structure of any input model. Under the guidance of the structure measurement, the envelope is computed in a structure-aware manner and the sharp features are well preserved. Unlike previous feature-preserving EMD methods for meshed models, our algorithm does not explicitly resort to sharp feature detection, which is more suitable for complex geometric models. With the well decomposed multi-scale representation, we could explore various applications of point clouds, such as detail enhancement and smoothing, feature points extraction, and feature-preserving denoising. We showcase comprehensive experimental results to demonstrate the utility of our novel multi-scale mesh-free EMD algorithm.

© 2017 Elsevier B.V. All rights reserved.

[☆] This paper has been recommended for acceptance by Marc Alexa.

* Corresponding author at: College of Sciences, Northeast Electric Power University, Jilin 132012, China.

E-mail addresses: wangxiaochao18@163.com (X. Wang), neduhjp307@163.com (J. Hu), guolx@buaa.edu.cn (L. Guo), zhangdongbo9212@163.com (D. Zhang), qin@cs.stonybrook.edu (H. Qin), ham@buaa.edu.cn (A. Hao).

1. Introduction

In digital geometry processing, point clouds are one of the most commonly-available types of data and they have been extensively employed to represent 3D shapes with the increasing availability of modern hardware devices and data acquisition technologies. The explosive growth of the data brings us more opportunities and challenges, as a result, more novel techniques are urgently needed for point clouds' analysis and processing. To date, empirical mode decomposition (EMD) has become a powerful and effective analytical tool for non-stationary, non-linear signals, which could decompose a signal into a number of intrinsic mode functions (IMFs) and could represent the signal at different scales ranging from higher-frequency to lower-frequency in a multi-scale manner. EMD is first proposed by [Huang et al. \(1998\)](#) and has shown its advantages in handling non-linear and non-stationary signals. Benefiting from the attractive properties, there are plenty of EMD-based methods that have been proposed in 1D signal processing ([Huang et al., 1998, 2003](#); [Kopsinis and McLaughlin, 2009](#); [Mandic et al., 2013](#); [Di et al., 2014](#)) and 2D image analysis ([G. Xu et al., 2009](#); [Subr et al., 2009](#); [Çelebi and Ertürk, 2012](#); [Niang et al., 2012](#); [Krinidis and Krinidis, 2013](#); [Xie, 2014](#); [Zang et al., 2014, 2015](#); [Ali et al., 2015](#)).

Recently, EMD has attracted much attention in computer graphics and a few EMD-based methods for triangular mesh are proposed in [Qin et al. \(2009\)](#), [H. Wang et al. \(2012\)](#), [Hu et al. \(2014, 2016\)](#), [Wang et al. \(2015, 2017\)](#), [Zhang et al. \(2017\)](#). Despite the fact that EMD has exhibited its potential in 3D mesh processing, extending the existing techniques of EMD to operate directly on point clouds remains to be extremely challenging. This is primarily because of the point clouds are unorganized without topological information.

Furthermore, for irregular, curved, and complex geometric models, sharp features are usually contained in point clouds, more efforts should be taken to preserve them during EMD-enabled geometry processing. The original EMD is conducted via the sifting process by iteratively computing the mean envelope of the signal, in such a way the sharp feature could not be preserved. In the literature, a few attempts have modified the original EMD to achieve a feature-preserving EMD-based algorithm on triangular meshes, such as [H. Wang et al. \(2012\)](#) which was seeking an interpolation by minimizing a quadratic function that measures the similarity between the current vertex with its neighbors. However, the proposed feature-aware interpolation method is not sufficiently robust. In [Hu et al. \(2014\)](#), Hu et al. explicitly detected the feature vertices as soft constraints during envelope computation. In another way, a divide-and-conquer scheme of EMD is proposed in [Wang et al. \(2015\)](#) by explicitly separating the feature signals from non-feature signals. However, they have a drawback that the effectiveness of feature-preserving heavily depends on the result of sharp feature detection. If the models are contaminated with heavy noise, and features are not faithfully extracted, unpleasant artifacts emerge and sharp features turn out to be absolutely blurred.

In this paper, in order to overcome these limitations, we propose a multi-scale mesh-free EMD algorithm directly functioning over point clouds without building explicit connectivity among discrete points. We further explore its widespread applications in geometry analysis and processing. The multi-scale mesh-free EMD is achieved by iteratively extracting the detail level from the input signal and leaving the overall shape in residue. Furthermore, in order to preserve sharp features during point-based EMD analysis/processing, we devise a new envelope computation scheme aided by an anisotropic structure measurement. Inspired by the work of [Zang et al. \(2015\)](#), [Park et al. \(2012\)](#), the structure measurement is first constructed from the unstructured point clouds by the eigenvalue decomposition of voting tensor, which could faithfully characterize the micro-structure of any input model. Under the guidance of the structure measurement, the envelope is computed in a structure-aware manner and the sharp features could be well preserved. Then, the mean envelope is computed by creating adaptive shocks near salient structures and the input signal of the scattered point clouds is the finally represented in a multi-scale manner with features preserved in residue. The pipeline of proposed EMD algorithm on point clouds is illustrated in [Fig. 1](#).

In comparison with previous works, the main contributions of this paper can be summarized as follows:

- Generalizing the classical EMD algorithm from Euclidean space to the setting of surfaces represented as unorganized point clouds, we are proposing the multi-scale mesh-free EMD. To the best of our knowledge, this is the first attempt to devise the EMD algorithm directly over discrete point clouds without the need of explicit mesh construction.
- Under the guidance of the structure measurement, we develop an efficient and novel feature-preserving EMD algorithm. Unlike previous feature-preserving EMD methods for meshed models, our algorithm does not explicitly resort to sharp feature detection, as a result, our new algorithm is more robust to noise and suitable for much more complicated point-based models.
- With the well decomposed multi-scale representation, we could explore various applications of point clouds, such as detail enhancement and smoothing, feature points extraction, and feature-preserving denoising, which collectively can demonstrate the utility of our novel multi-scale mesh-free EMD algorithm.

2. Related work

EMD is an important multi-scale decomposition method and initially proposed by [Huang et al. \(1998\)](#). In this section, we briefly introduce the related work of EMD on Euclidean space, 3D surfaces, and the feature-preserving EMD.

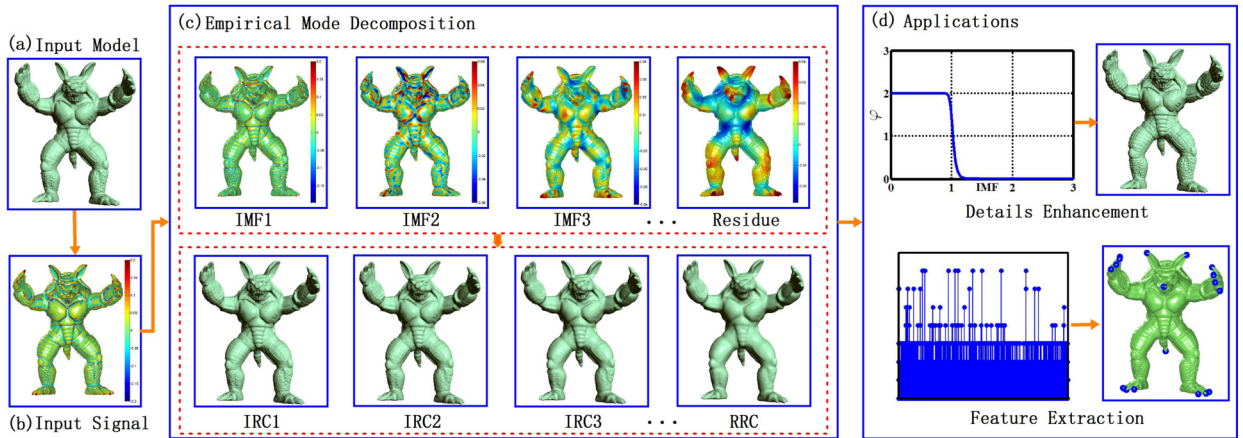


Fig. 1. Mesh-free empirical mode decomposition on point clouds. (a) Original model. (b) Input signal defined in Eq. (2). (c) Empirical mode decomposition. Top: IMFs and the residue. Bottom: The models corresponding to IMFs are reconstructed using its IMFs together with the residue, and are denoted as IRCs and RRC. For visualization, the models are shown in surfaces by utilizing the ball pivoting algorithm (Bernardini et al., 1999). (d) The applications of geometry detail enhancement and feature point extraction.

2.1. EMD on Euclidean space

The original EMD is designed for 1D signal processing, especially for nonlinear and non-stationary signals. By using this decomposition algorithm, the given signal can be represented as different scale oscillatory modes. Comparing with traditional time-frequency analysis methods, such as Fourier and wavelet analysis, EMD is fully data-driven and does not depend on any predefined basis functions. Benefiting from its elegant property, EMD has been broadly applied in 1D signal analysis and processing (Huang et al., 1998, 2003; Kopsinis and McLaughlin, 2009; Mandic et al., 2013; Di et al., 2014; Luo et al., 2003; Gemmrich and Farmer, 2004; Wu et al., 2008; Schneider et al., 2009).

In addition, EMD has been generalized to process the high-dimensional signals defined on regular domains, such as 2D images and 3D volume data (Linderhed, 2002; Nunes et al., 2003; Xu et al., 2006; Long, 2005; Wu et al., 2009; Gao et al., 2013). The critical problem of such generalization is how to compute envelopes, which interpolate the extrema of the signal during the sifting process. Linderhed (2002) used a thin-plate spline for surface interpolation to develop 2D EMD algorithm for an image compression scheme. Nunes et al. (2003) generated envelope surfaces by radial basis function interpolation and used the Riesz transform for image analysis. Xu et al. (2006) directly used a mesh fitting method based on bi-cubic spline interpolation to compute the local mean surface of 2D data directly. Long (2005) processed each row or each column of 2D image data respectively by 1D EMD. Wu et al. (2009) proposed a similar slice approach to reduce the high-dimensional data into 1D data. In volume data processing, following the idea of dimensionality reduction, Gao et al. (2013) firstly used Hilbert curve to flatten 3D data into 1D signal, and then decomposed the 1D signal by the classical 1D EMD method. Following this way, Ren et al. (2013) computed spatial Hilbert spectrum on 3D fluid data by 1D Hilbert transform after transforming the signal to 1D signal, which is applied in flow field modulation.

2.2. EMD on 3D surfaces

Different from the regular domains in Euclidean space, 3D surfaces are irregular, curved, and possibly have complex structure, which further give rise to new challenges for EMD generalization on 3D geometry processing. The EMD based fairing algorithm for meshed surface was proposed by Qin et al. (2009), in which the spherical parameterization is used to transform the 3D surface signal to a 2D planar signal, then decompose the signal using the 2D EMD algorithm. However, the spherical parameterization prevents its further application to more complex surfaces in topology. To address this issue, an alternative algorithm based on bi-harmonic interpolation was proposed by H. Wang et al. (2012) and further employed in the work of Hu et al. (2014). In addition, in order to speed up the EMD on mesh processing, Wang et al. (2015) proposed an accelerating algorithm via the strategy of dimensionality reduction and explicitly utilized the concept of space filling curve. To our best knowledge, EMD algorithms have not yet appeared in point cloud processing.

2.3. Feature-preserving EMD

Due to the over-smoothing effect inheriting from the original EMD, the sharp feature could not be preserved both in 2D images and 3D surfaces. To achieve feature-preserving image smoothing, a joint contrast-based filtering step for structure consolidation is applied on the result of empirical mode decomposition in Zang et al. (2014). Despite the fact that the post-processing step is adopted, blur effects still occur along salient edges. This problem is further addressed by restoring to extend extreme and structure measurement in Zang et al. (2015).

In 3D geometry processing, inspired by the extreme-based image smoothing (Subr et al., 2009), H. Wang et al. (2012) resorted to an interpolation by minimizing a quadratic function with an edge-aware Laplace operator, which measures the similarity between the current vertex and its neighbors. However, the proposed feature-aware interpolation method is not sufficiently robust. In Hu et al. (2014), Hu et al. explicitly detected the sharp feature vertices as soft constraints in envelope computation. Similarly, a divide-and-conquer scheme of EMD is proposed in Wang et al. (2015) by explicitly separating the feature signals from non-feature signals. Either applying the post-processing (Zang et al., 2014) or using the explicit feature vertices as constraints (Hu et al., 2014; Wang et al., 2015), our observation is that, the feature-preserving property of EMD has not yet been essentially achieved. More importantly, the experimental results are sensitive to the accuracy of feature detection. If features are not properly or precisely extracted, unpleasant artifacts will emerge and sharp features will be blurred.

3. EMD on point clouds

In this section, the original 1D EMD is illustrated briefly and then its direct extension to 3D point clouds is introduced.

3.1. The original 1D EMD

The original 1D EMD was first developed by Huang et al. (1998) and was designed for 1D signal processing. The main idea of EMD is decomposing a signal into a finite number of intrinsic mode functions (IMFs), where the first IMF starts with the finest scale, and the subsequent IMFs gradually exhibit coarse scales. The IMFs represent the natural oscillatory modes embedded in signals and play a role of the basis functions, which can be obtained by a sifting process. In this process, the extrema are first identified for a given signal X , and then the upper and lower envelopes are computed from the maxima and minima by a cubic spline, separately. Next, the difference $h_1 = X - m_0$ between the input signal X with the mean envelope m_0 is defined as the first IMF, if it satisfies the stopping criterion of an IMF. Otherwise, h_1 is treated as the input data, and repeat the above process.

Denote the first IMF as d_1 , and set $r_1 = X - d_1$ as the first residue. The second IMF is extracted by repeating the sifting process to the first residue r_1 . This process will be terminated if the residue becomes a constant or monotonic function or the number of IMFs is more than a given threshold. The sifting process serves as two purposes: to eliminate riding waves and to make the wave-profiles more symmetric (Huang et al., 1998). Finally, the input signal X is presented as

$$X = \sum_{i=1}^N d_i + r_N, \quad (1)$$

where N is the total number of IMFs, and r_N is the final residue of the input signal X . The sifting process of EMD on 1D signal is illustrated in Fig. 2. More details of EMD can be found in Huang et al. (1998), H. Wang et al. (2012), Hu et al. (2014), Wang et al. (2015).

3.2. 3D EMD on point clouds

Given a point set $P = \{\mathbf{p}_i, i = 1, \dots, n\}$ sampled from an unknown manifold S , the signal should be defined first in EMD-based point clouds processing. The signal \mathbf{f} defined on point clouds either represents the original geometry shape or characterizes the geometry feature of the input model, which could be simple geometric coordinates of point clouds, normal function, certain variant of curvature measurement, height field over some base surface. In our work, the signal is defined by the inner product of Laplacian coordinate with the corresponding point normal

$$\mathbf{f}(\mathbf{p}_i) = \mathbf{n}(\mathbf{p}_i) \cdot \delta(\mathbf{p}_i), \quad (2)$$

which could be regarded as a direct height field defined over the smoothed point clouds via Laplacian-based smoothing. The normal of point clouds can be estimated and orientated by the algorithm of Liu et al. (2014).

The Laplacian coordinate δ_i is calculated by

$$\delta_i = \sum_{\mathbf{p}_j \in N(\mathbf{p}_i)} w_{ij}(\mathbf{p}_j - \mathbf{p}_i), \quad (3)$$

where $N(\mathbf{p}_i)$ is the set of the neighbor points of \mathbf{p}_i and w_{ij} is defined by Gaussian weight

$$w_{ij} = \frac{1}{4\pi\alpha^2} \exp\left(-\frac{\|\mathbf{p}_i - \mathbf{p}_j\|^2}{4\alpha}\right), \quad (4)$$

with the parameter α to control the influence region. The signal is rotation-invariant, translation-invariant, and can be used as the input in EMD-based point cloud processing.

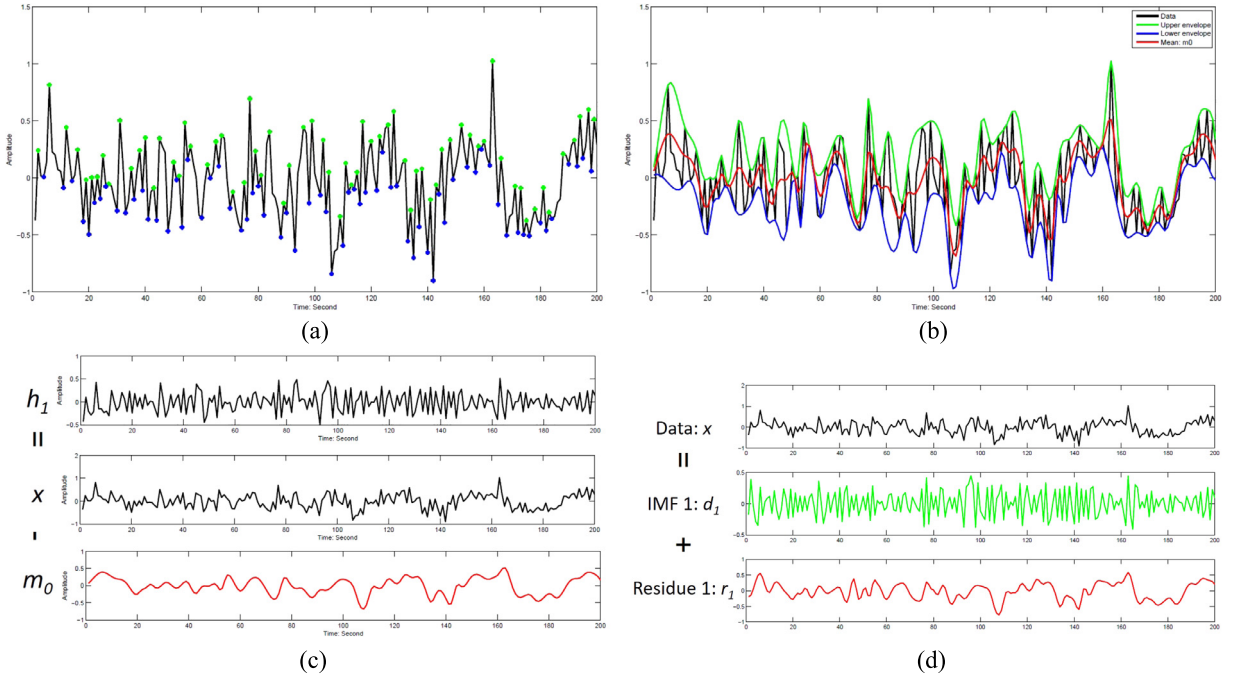


Fig. 2. Illustration of sifting process on 1D signal. (a) Input signal and detected maximum points (green) and minimum points (blue). (b) The computed upper (green), lower (blue) and mean envelopes (red). (c) The difference between the input signal with the mean envelope. (d) The input signal is decomposed into a first IMF and a residue. (For interpretation of the references to color in this figure legend, the reader is referred to the web version of this article.)

Algorithm 1 EMD on point clouds.

Input: A signal \mathbf{f} defined on point clouds

Output: IMFs $\mathbf{h}_k, k = 1, \dots, d$ and a residue \mathbf{r}_d

Initialization: Set $k = 1$ and initial residue $\mathbf{r}_0 = \mathbf{f}$;

1: **repeat**

2: $\mathbf{s}_0 = \mathbf{r}_{k-1}, i = 1$;

3: **for each** i **do**

4: Find local minima and local maxima of \mathbf{s}_{i-1} ;

5: Compute the lower envelope \mathbf{l}_{i-1} and upper envelope \mathbf{u}_{i-1} by interpolating all local minima and maxima by solving the bi-harmonic field with Dirichlet boundary conditions;

6: Compute the mean envelope \mathbf{m}_{i-1} of \mathbf{s}_{i-1} by $\mathbf{m}_{i-1} = (\mathbf{l}_{i-1} + \mathbf{u}_{i-1})/2$;

7: $\mathbf{s}_i = \mathbf{s}_{i-1} - \mathbf{m}_{i-1}$;

8: **if** \mathbf{s}_i satisfies the stopping criterion **then**

9: Get the k -th IMF $\mathbf{h}_k = \mathbf{s}_i$ and the k -th residue $\mathbf{r}_k = \mathbf{r}_{k-1} - \mathbf{h}_k$;

10: $k = k + 1$;

11: **break**;

12: **else**

13: $i = i + 1$;

14: **end if**

15: **end for**

16: **until** The residue is a constant or monotonic function or the number of IMFs is larger than a user-specified value

For the signal \mathbf{f} defined on points of P , it can be decomposed into multi-scale representation via EMD algorithm

$$\mathbf{f} = \sum_{i=1}^d \mathbf{h}_i + \mathbf{r}_d, \quad (5)$$

where \mathbf{h}_i is the i -th IMF of \mathbf{f} , and \mathbf{r}_d is the residue of the signal. Usually, the leading IMFs represent the fine details of a signal, while the trailing IMFs encodes the smooth shape of a model. The algorithm of EMD on point clouds involves three main steps of local extrema identification, envelope computation, and stopping criteria, which is briefly presented in Algorithm 1.

Extremum identification. For point clouds, the topology information is unavailable, a maximum/minimum of a signal is defined in the following, which will be used as an anchor in envelope computation.

- \mathbf{p}_i is a maximum if $\mathbf{f}(\mathbf{p}_i) \geq \mathbf{f}(\mathbf{p}_j), \mathbf{p}_j \in N(\mathbf{p}_i)$

- \mathbf{p}_i is a minimum if $\mathbf{f}(\mathbf{p}_i) \leq \mathbf{f}(\mathbf{p}_j)$, $\mathbf{p}_j \in N(\mathbf{p}_i)$

Envelope computation. To compute the envelope from the local extrema of the signal on S , the interpolation method by minimizing the linearized thin-plate energy is adopted (H. Wang et al., 2012)

$$\int_S (\Delta_S \mathbf{f})^2 dP, \quad (6)$$

which defines a measure of smoothness of \mathbf{f} and the corresponding Euler–Lagrange equation of the energy is

$$\Delta_S^2 \mathbf{f} = 0, \quad (7)$$

where Δ_S is the Laplace–Beltrami operator of surface S .

For point clouds P , there are several ways to construct the discrete Laplacian for point clouds (Belkin et al., 2009; Luo et al., 2009; Luo, 2014). In this work, the Voronoi–Laplacian proposed by Luo et al. (2009), Luo (2014) is adopted with the elements of the Laplacian matrix being

$$\mathbf{L}_{ij} = \begin{cases} w_{ij} A_j, & \text{if } i \neq j \\ w_{ii} A_i - \sum_{j=1}^n w_{ij} A_j, & \text{if } \textit{otherwise} \end{cases}, \quad (8)$$

where A_i is the Voronoi weight of point \mathbf{p}_i , which roughly accounts for the area of the underlying manifold represented by the sample point \mathbf{p}_i and can be calculated by considering the points within a certain distance around point \mathbf{p}_i . The weight w_{ij} is computed in Eq. (4).

To obtain the interpolation function $\mathbf{g} = (\mathbf{g}(\mathbf{p}_1), \mathbf{g}(\mathbf{p}_2), \dots, \mathbf{g}(\mathbf{p}_n))$ with the interpolated anchors and corresponding values $\{(\mathbf{p}_i, \mathbf{f}_i), i \in \Lambda\}$, a sparse $n \times n$ linear system is constructed

$$\mathbf{L}^2 \mathbf{g} = 0, \quad \text{s.t. } \mathbf{g}(\mathbf{p}_i) = \mathbf{f}(\mathbf{p}_i), \quad i \in \Lambda, \quad (9)$$

where Λ is the set of interpolated anchors for the signal \mathbf{f} and this system can be solved by the direct elimination method (K. Xu et al., 2009).

Stopping criteria of the sifting process and the entire EMD processing. Following the computational strategy of the original 1D EMD, the stopping criteria of the sifting process of EMD on point clouds is controlled by restricting the size of the standard deviation

$$SD = \sum_{t=1}^n \frac{|\mathbf{s}_{i-1}(\mathbf{p}_t) - \mathbf{s}_i(\mathbf{p}_t)|^2}{|\mathbf{s}_{i-1}(\mathbf{p}_t)|^2}, \quad (10)$$

with \mathbf{s}_{i-1} and \mathbf{s}_i are two consecutive sifting functions in one iteration. The smaller the value is, the more IMFs we will obtain. The typical value of SD is set in the range of 0.1 to 0.3.

The entire EMD process will be terminated when either the component \mathbf{h}_k or the residue \mathbf{r}_k becomes so small that it is less than the pre-determined value of substantial consequence, or the residue \mathbf{r}_k becomes a monotonic function from which no more IMFs could be extracted (Huang et al., 1998). In practice, the process of EMD can be stopped when the number of IMFs is larger than a pre-determined threshold or the numbers of local minima and maxima of the residue is smaller than the user specified value.

Surface reconstruction. According to different requirements of various applications, such as smoothing, detail enhancing and denoising, the decomposed IMFs are modified to generate a new signal \mathbf{f}' . The processed point clouds with new point $P' = \{\mathbf{p}'_i, i = 1, \dots, n\}$, corresponding to the new signal \mathbf{f}' can be reconstructed in the least-squares sense with the original points $P = \{\mathbf{p}_i, i = 1, \dots, n\}$ as constraints. The reconstruction process is enabled by minimizing the following energy

$$\|\mathbf{L}\mathbf{P}' - \text{diag}(\mathbf{f}')\mathbf{N}\|^2 + \tau^2 \sum_{i=1}^n \|\mathbf{p}'_i - \mathbf{p}_i\|^2, \quad (11)$$

where $\text{diag}(\mathbf{f}')$ returns a square diagonal matrix with the elements of vector \mathbf{f}' on the main diagonal and the parameter τ is a weight of original points, the default value is set to be 0.01, and \mathbf{N} is the point normal matrix and \mathbf{L} is the Laplacian matrix.

Minimizing the energy of Eq. (11), a linear system is obtained,

$$\begin{bmatrix} \mathbf{L} \\ \tau \mathbf{I}_{n \times n} \end{bmatrix} \mathbf{P}' = \begin{bmatrix} \text{diag}(\mathbf{f}')\mathbf{N} \\ \tau \mathbf{P} \end{bmatrix}, \quad (12)$$

then it can be efficiently solved in the least-squares sense with $\mathbf{A}^T \mathbf{A} \tilde{\mathbf{V}} = \mathbf{A}^T \mathbf{b}$ by Cholesky factorization.

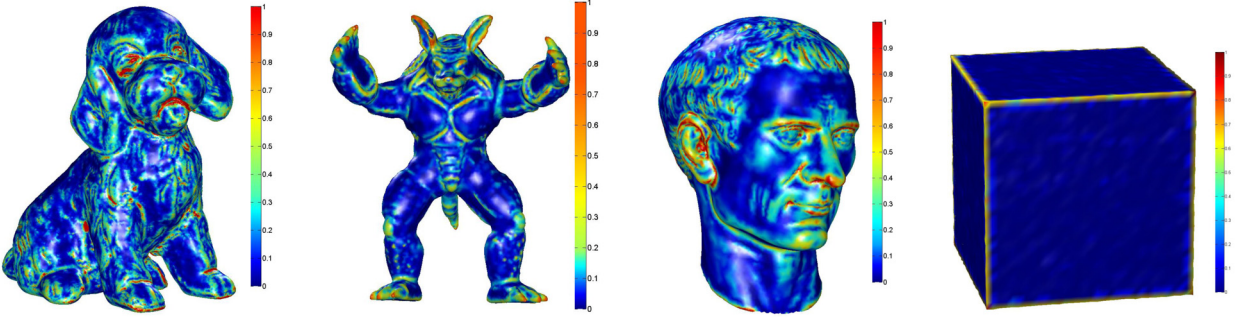


Fig. 3. The map of structure measurement on different models. (For interpretation of the references to color in this figure, the reader is referred to the web version of this article.)

4. Feature-preserving EMD on point clouds

In geometry processing, sharp features have been playing an important role in shape modeling, representation, reconstruction, and should be completely preserved during data processing. However, directly extending the original EMD from 1D signal to deal with 3D point clouds could not preserve the sharp features well. To overcome this limitation, we further improve the algorithm presented in the previous section to achieve a feature-preserving EMD algorithm on point clouds under the assistance of the structure measurement.

4.1. Structure measurement and its computation

For characterizing the feature structure of input point clouds, we seek to define the structure measurement via tensor voting theory, which has been widely used for feature and saliency detection in images (Zang et al., 2015; Baghaie and Yu, 2006; Manh et al., 2015), triangular meshes (Tsuchie and Higashi, 2012; Kim et al., 2009; X. Wang et al., 2012) and point clouds (Park et al., 2012). The tensor voting is a powerful and robust technique for feature and saliency detection. Motivated by these works, we utilize the tensor voting theory to describe the feature structure of point clouds and integrate the structure measurement into the EMD algorithm to achieve the feature-preserving EMD algorithm on point clouds.

Tensor voting for point clouds. To calculate the structure measurement, the voting tensors are first collected from the neighboring points, which encode the underlying geometry information in the local region. Specifically, for a point \mathbf{p}_i and its neighbor point \mathbf{p}_j , the voting tensor $\mathbf{T}_{\mathbf{p}_i}$ of point \mathbf{p}_i is obtained by integrating the weighted covariance matrices of its neighbor points

$$\mathbf{T}_{\mathbf{p}_i} = \sum_{\mathbf{p}_j \in N(\mathbf{p}_i)} \mu_j \cdot (\mathbf{p}_i - \mathbf{p}_j) \cdot (\mathbf{p}_i - \mathbf{p}_j)^T = \sum_{\mathbf{p}_j \in N(\mathbf{p}_i)} \mu_j \cdot \mathbf{T}_{ij}, \quad (13)$$

where $N(\mathbf{p}_i)$ is the set of neighborhood of point \mathbf{p}_i and μ is the weight measuring the contribution of each point to the voting procedure, which is decided by the distance between the point and its neighbors. Oftentimes, the Gaussian function is utilized

$$\mu_j = \exp(-\|\mathbf{p}_i - \mathbf{p}_j\|^2 / \theta^2), \quad (14)$$

with the parameter θ to control the influence of propagation range. The parameter θ should be adjusted based on the degree of noise contained in the model. For noise-free models, the smaller value will be used, while a larger value will be adopted for the models contaminated with heavy noise. In practice, we find that θ ranging from 1.5 to 3 times the mean nearest-neighbor distance of the point clouds accommodates well for the experiments shown in this paper.

Voting analysis. According to Eq. (13), the voting tensor is a symmetric positive semi-definite second-order tensor, therefore, it can be reorganized by using its eigen-values and eigen-vectors as

$$\mathbf{T}_{\mathbf{p}_i} = \lambda_1 \mathbf{e}_1 \mathbf{e}_1^T + \lambda_2 \mathbf{e}_2 \mathbf{e}_2^T + \lambda_3 \mathbf{e}_3 \mathbf{e}_3^T, \quad (15)$$

where $\mathbf{e}_1, \mathbf{e}_2, \mathbf{e}_3$ are the eigen-vectors corresponding to the eigen-values $\lambda_1, \lambda_2, \lambda_3$ with $\lambda_1 \geq \lambda_2 \geq \lambda_3 \geq 0$.

After the tensor decomposition, the structure measurement is computed as (Park et al., 2012)

$$D_{\mathbf{p}_i} = \frac{\lambda_2 + \lambda_3}{\lambda_1}, \quad (16)$$

which measures the intrinsic feature intensity of each point and is normalized to the range of [0, 1]. The value of the measure is very small in flat region and increases for the point locating on sharp and detail regions. Fig. 3 shows the saliency measurement map of different models, including both organic models and a mechanical CAD model, in which the structures are faithfully described.

4.2. Feature-preserving EMD algorithm on point clouds

To overcome the limitation of EMD and preserve the sharp features, the structure measurement is integrated into the process of EMD as the guidance in envelope computation and mean envelope computation.

4.2.1. Envelope computation

Following the idea of envelope computation of EMD on triangular meshes, bi-harmonic interpolation is used to generate the upper and lower envelopes in present of point clouds. Unlike previous methods (Hu et al., 2014; Wang et al., 2015), where the feature vertices are explicitly detected in advance, we utilize the structure measurement to construct the anisotropic point cloud Laplacian matrix.

The anisotropic Laplacian matrix \mathbf{L} is computed in Eq. (8) by integrating the structure measurement as feature-aware weight

$$w_{ij} = \frac{1}{4\pi\alpha^2} \exp\left(-\frac{\|\mathbf{p}_i - \mathbf{p}_j\|^2}{4\alpha}\right) \exp\left(-\frac{|D_{\mathbf{p}_i} - D_{\mathbf{p}_j}|^2}{2\beta^2}\right), \quad (17)$$

where D is the structure measurement computed in Eq. (16) and β is the local standard deviation of D in its neighborhoods.

With the interpolated anchors and corresponding values $(\mathbf{p}_i, \mathbf{f}_i), i \in \Lambda$, the values of interpolation function at vertices $\mathbf{g} = (\mathbf{g}(\mathbf{p}_1), \mathbf{g}(\mathbf{p}_2), \dots, \mathbf{g}(\mathbf{p}_n))$ can be obtained by minimizing the following energy function

$$\|\mathbf{L}\mathbf{f}\|^2 + \mu^2 \sum_{\mathbf{p}_j \in N(\mathbf{p}_i)} |\mathbf{g}(\mathbf{p}_i) - \mathbf{f}(\mathbf{p}_j)|^2, \quad (18)$$

with the interpolated anchor constraints

$$\mathbf{g}(\mathbf{p}_i) = \mathbf{f}(\mathbf{p}_i), \quad i \in \Lambda, \quad (19)$$

where μ is the weight factor for balancing the smoothing term and the interpolated term, and the default value is set to be 0.1 in all of our experiments.

4.2.2. Mean envelope computation

An important reason that the original EMD could not preserve sharp feature is largely due to the mean envelope computation scheme, in which the mean envelope is calculated by simply averaging the upper and lower envelopes and thus results in feature blurring. Therefore, we expect to further improve the mean envelope computation scheme in order to design a feature-preserving EMD algorithm on point clouds.

Inspired by the work of Zang et al. (2015), Weickert (2003), we compute the mean envelope using *shock filter* (Osher and Rudin, 1990; Kramer and Bruckner, 1975; Prada, 2015) with the help of the structure measurement defined in this paper. The *shock filter* was first proposed by Kramer and Bruckner (1975) for image enhancement and it has been further used in geometry processing (Prada, 2015). The goal of the *shock filter* is to produce the sharp discontinuity at the borderline between different influence regions. Under the guidance of structure measurement and the scheme of *shock filter*, the mean envelope is computed by

$$\begin{aligned} \mathbf{m}(\mathbf{p}_i) = & \Gamma\left(\frac{1 - \text{sign}(\mathbf{n}_i \cdot \delta_i) \cdot D(\mathbf{p}_i)}{2}\right) \mathbf{u}(\mathbf{p}_i) \\ & + \left(1 - \Gamma\left(\frac{1 - \text{sign}(\mathbf{n}_i \cdot \delta_i) \cdot D(\mathbf{p}_i)}{2}\right)\right) \mathbf{l}(\mathbf{p}_i), \end{aligned} \quad (20)$$

where \mathbf{l} and \mathbf{u} are the lower and upper envelopes of the signal \mathbf{f} , respectively. D is the structure measurement computed in Eq. (16). $\text{sign}(\cdot)$ is determined by the inner product of the normal \mathbf{n}_i and the Laplacian coordinate δ_i of point \mathbf{p}_i . In practice, for noisy point clouds, $\text{sign}(\cdot)$ is computed on an over smoothed data to reduce the effect of noise.

The degree of *shock filter* is measured by the function $\Gamma(\cdot)$ and is defined by the following function

$$\Gamma(x) = \frac{1 + \tanh(\gamma(x - 0.5))}{2}, \quad (21)$$

with parameter γ to control its sharpness. Usually, the larger the γ is, the sharper result will be obtained. In our experiments the default value of γ is set to 6 for sharp feature preserving.

The ultimate goal of the newly developed mean envelope computation scheme is to preserve sharp feature. In feature region, the structure measurement lies in larger value and approximates to 1, the mean envelope \mathbf{m} approaches to

$$\mathbf{m}(\mathbf{p}_i) = \begin{cases} \mathbf{u}(\mathbf{p}_i) & \text{if } \text{sign}(\mathbf{p}_i) < 0, \\ (\mathbf{u}(\mathbf{p}_i) + \mathbf{l}(\mathbf{p}_i))/2 & \text{if } \text{sign}(\mathbf{p}_i) = 0, \\ \mathbf{l}(\mathbf{p}_i) & \text{if } \text{sign}(\mathbf{p}_i) > 0, \end{cases} \quad (22)$$

Algorithm 2 Multi-scale feature-aware EMD on point clouds.**Input:** A signal \mathbf{f} defined on point clouds**Output:** IMFs $\mathbf{h}_k, k = 1, \dots, d$ and a residue \mathbf{r}_d **Initialization:** Set the index of IMFs $k = 1$ and initial residue $\mathbf{r}_0 = \mathbf{f}$;

- 1: **repeat**
- 2: Find local minima and local maxima of \mathbf{r}_{k-1} ;
- 3: Compute the structure measurement by Eq. (16) and discrete Laplacian operator for point clouds by Eq. (8) with the feature-aware weight by Eq. (17);
- 4: Compute the lower envelope \mathbf{l}_{k-1} and upper envelope \mathbf{u}_{k-1} using Eq. (18);
- 5: Compute the mean envelope \mathbf{m}_{k-1} using the *shock filter* by Eq. (20);
- 6: Extract the k -th level \mathbf{h}_k by $\mathbf{h}_k = \mathbf{r}_{k-1} - \mathbf{m}_{k-1}$ and set the k -th residue by $\mathbf{r}_k = \mathbf{m}_{k-1}$;
- 7: $k = k + 1$;
- 8: **until** The number of levels reaches a user-specified number

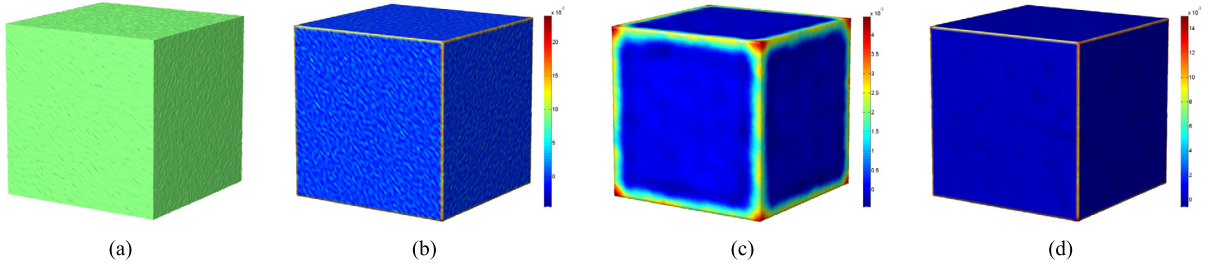


Fig. 4. Illustration of the processed signal on a cube mode. (a) A cube model corrupted with Gaussian noise of 5% of average distance between neighboring points. (b) Input signal. (c) and (d) are residue obtained by EMD without and with structure measurement assistance, respectively. (For interpretation of the references to color in this figure, the reader is referred to the web version of this article.)

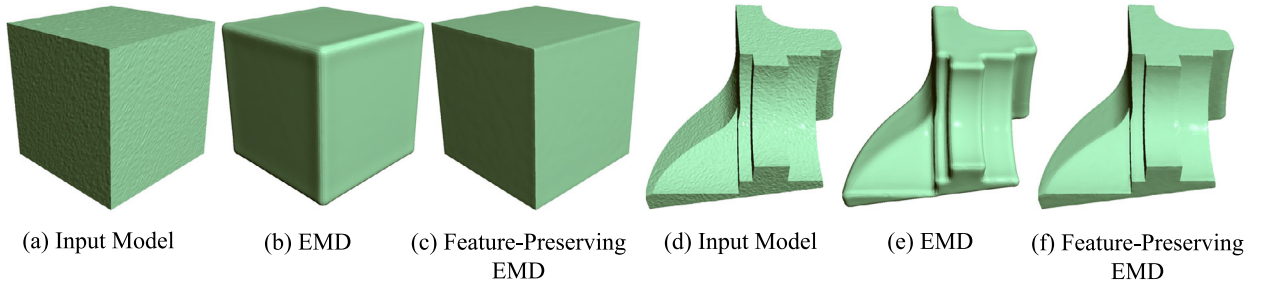


Fig. 5. Illustration of feature-preserving EMD algorithm. (a) and (d) are input cube and Fandisk model. (b) and (e) are denoising results by using EMD. (c) and (f) are denoising results using feature-preserving EMD.

with the feature effectively preserved. On the other hand, in smooth and flattened regions, the value of structure measurement D is close to 0, then Eq. (20) degrades to the conventional definition of mean envelope $(\mathbf{u} + \mathbf{l})/2$.

To accelerate the decomposition process, following the scheme of the work (Subr et al., 2009; Hu et al., 2014), our decomposition algorithm obtains the detail level by subtracting the mean envelope from the input signal instead of the iterative sifting process. The multi-scale representation will be obtained by repeating the process until reaching the required number of levels. The algorithm of our feature-preserving EMD on point clouds is summarized in Algorithm 2. Fig. 4 illustrates the decomposition results of EMD on a noisy cube. From Fig. 4(c) and Fig. 4(d), it is evident that the EMD with structure measurement assistance achieves much clearer feature preserving in the residue than the EMD without structure measurement assistance. Furthermore, Fig. 5 shows the results using EMD and feature-preserving EMD. From the results, we can see that the sharp features are smoothed using the EMD algorithm, while they are well preserved using the feature-preserving EMD.

5. Experimental results and applications

In this section, the applications of point clouds including detail smoothing and enhancing, feature point extraction, as well as feature-preserved denoising, are shown to illustrate the efficiency and performance of our proposed EMD algorithm on point clouds. The algorithm is evaluated on both synthetic and real scanned point clouds, and the results are shown in surfaces reconstructed from the corresponding point clouds by the ball pivoting algorithm (Bernardini et al., 1999).

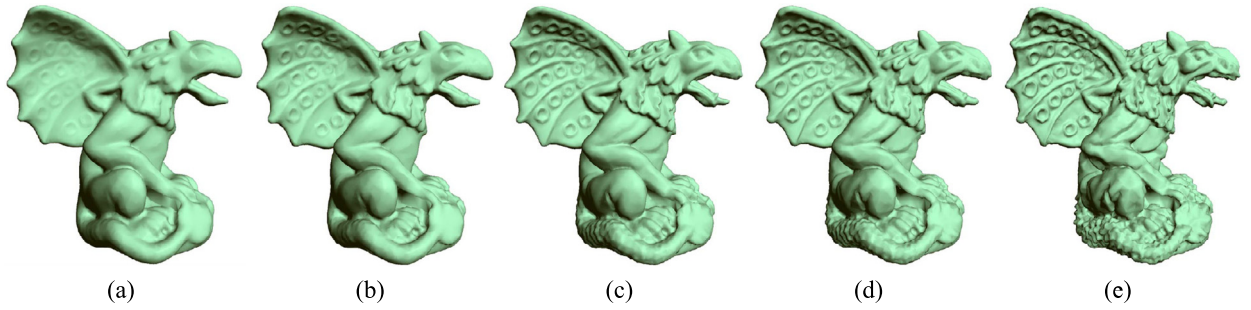


Fig. 6. Smoothing and enhancing results of Gargo model. (a) The smoothing result reconstructed from the residue. (b) The smoothing result with the scaling coefficients (0, 0, 1). (c) The original model. (d–e) The enhancing results with scaling coefficients (2, 1, 1) and (4, 1, 1), respectively.

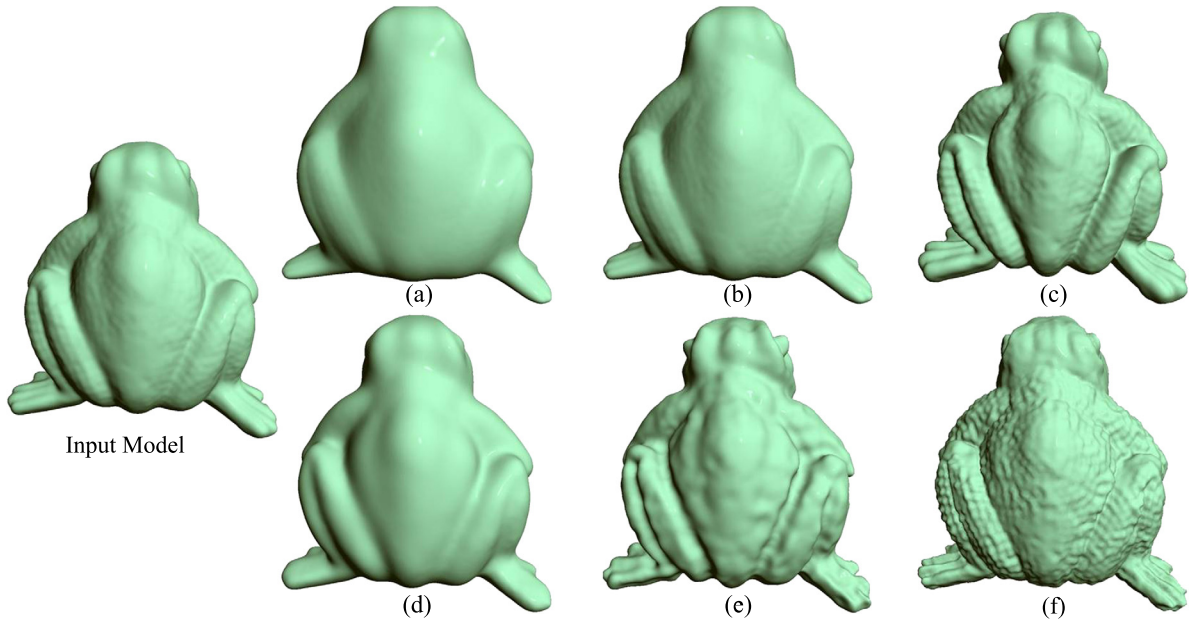


Fig. 7. Comparing results between our method with the Laplace-based detail modification method. (a–c) Laplace-based results from smoothing to enhancing. (d–f) Our results, which are obtained from the residue with parameter $\varphi_i = (0, 0, 0, 0, 0)$, enhancing the middle-scale with $\varphi_i = (0, 4, 4, 4, 0)$, enhancing the first IMFs with $\varphi_i = (5, 0, 0, 0, 0)$, respectively.

5.1. Detail smoothing and enhancing

As stated above, the leading IMFs encode the fine scale details and the trailing IMFs contain the smoother shape of the signal. Therefore, it is natural to execute the enhancing and smoothing filters by scaling corresponding IMFs with the residue unchanged,

$$\mathbf{f}' = \sum_{i=1}^d \varphi_i \mathbf{h}_i + \mathbf{r}_d, \quad (23)$$

where φ_i is the scaling coefficient with $\varphi > 1$ for enhancing and $0 \leq \varphi < 1$ for smoothing. In the following experiments, the signal is usually decomposed into three IMFs by the algorithm of point clouds EMD in the applications of smoothing and detail enhancing.

Benefiting from the multi-scale representation of EMD, smoothing and detail enhancing can be easily carried out on point clouds. Fig. 6 shows the results from smoothing to enhancing on Gargo model. Fig. 6(a) is the smoothing result reconstructed from the residue, in which the general outline of the shape is presented with details smoothed out. With the third IMF added, the detail features of the data appear gradually. Fig. 6(d–e) give the two enhancing results with the IMFs scaled by the factors (2, 1, 1) and (4, 1, 1), respectively. From these figures we can see that the detail features are apparently enhanced. These results further confirm that the detail features are encoded in the leading IMFs.

In Fig. 7, we compared our method with Laplace-based algorithm in detail modification on a frog model. To modify the details based on Laplace-based framework, we first compute the Laplacian coordinates of the model, then modify the

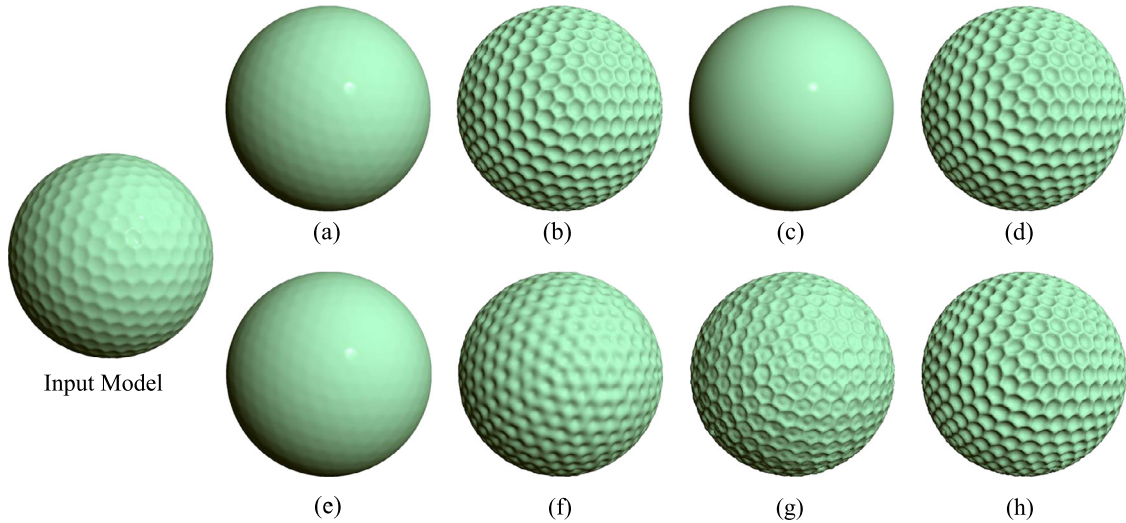


Fig. 8. Comparing EMD with MHBs (Vallet and Lévy, 2008) and SGWs (Hammond et al., 2011) for the detail editing. (a)–(b) The MHB-based results with editing coefficient $\{0\}$, $\{4\}$ for the detail extracted by separating the low frequency component in MHBs from the original signal, respectively. (c)–(d) The SGWs-based results with editing coefficient $\{0\}$, $\{4\}$ for the detail extracted by separating the wavelet representations in SGWs from the original signal, respectively. (e)–(h) Our results with parameter $\varphi_i = (0, 0, 0, 0, 0, 0)$, $(0, 4, 4, 4, 4, 0)$, $(5, 0, 0, 0, 5, 5)$, $(5, 5, 5, 5, 5, 0)$ for the decomposed five IMFs, respectively.

Laplacian coordinates by multiplying different scale values. Finally, the geometry shapes are reconstructed from the modified Laplacian coordinates via Laplacian framework. Fig. 7(a–c) are the results from smoothing to enhancing with scale values 0.2, 0.5, and 2.0, respectively. In our algorithm, we first decompose the signal into five IMFs and a residue, then the multi-scale detail modifications can be obtained by using different IMFs together with the residue. Fig. 7(d) is the smoothing result reconstructed from the residue. Fig. 7(e) is the middle-scale enhancing result obtained by enhancing the second to fourth IMFs with five times. Fig. 7(f) is the detail enhancing result with five times of the first IMFs. From the results we can see that Laplacian-based method can obtain the detail modifications from smoothing to enhancing. However, it is hard to modify the different scale details. In contrast, benefitting from the multi-scale decomposition of EMD, our method can easily and effectively modify different scale details, which can be seen from Fig. 7(d–f).

Furthermore, to demonstrate the advantage of EMD, we conducted some detail editing experiments to compare EMD with the well known manifold harmonic bases (MHBs) (Vallet and Lévy, 2008) and spectral graph wavelets (SGWs) (Hammond et al., 2011). MHBs are the eigenvectors of the Laplacians as the “Fourier-like” bases and the corresponding eigenvalues describe the space frequency of 3D models. SGWs are defined as bivariate kernel functions with the time and Laplacian eigenvalue variables expanded on the manifold harmonic bases where the time variable represents the scale parameter. Unfortunately, both of these two methods need a massive number of eigenvectors to describe high frequency detail information. For example, in the detail editing of 3D model with more than 120,000 vertices (Fig. 8), the eigenvectors corresponding to the smallest 1000 eigenvalues of the mesh Laplacians in MHB can only describe the low frequency information, and SGWs in the time interval $[2/\lambda_{max}, 40/\lambda_{max}]$ selected in Hammond et al. (2011) can not well represent the detail information using these eigenvectors either, where λ_{max} is the upper bound of the Laplacian eigenvalues. Obviously, it is impractical for large-sized models to compute a massive number of eigenvectors due to the limitation of physical memory and computational efficiency. Therefore, in our comparisons, we described the details of a 3D model according to the signal residue by separating the low frequency component in MHBs and the wavelet representations in the above time interval in SGWs from the original signal respectively (1000 eigenvectors are used in the eigenvalue decomposition). Accordingly, MHBs and SGWs based on the small amount of eigenvalue decomposition can only regard the modified details as one scale. As shown in Fig. 8, the results generated by these three methods are almost similar if the modified details are only edited in one scale. However, when adding more multi-scale controls, our method can generate more meaningful detail editing results (Fig. 8(e)–(h)) owing to the adaptive multi-scale representation ability of EMD for the geometry details.

5.2. Feature points detection

Our proposed EMD-based algorithm can also be applied to feature detection on point clouds. As demonstrated in the above sections, EMD decomposes the signal into multi-scale representation with IMFs encoding features of different scales. Therefore, the feature points can be extracted from the local extrema of each IMF. In general, more feature points will appear at the leading IMFs, and the number of feature points decreases in the subsequent IMFs. That is to say, some feature points extracted in the first few IMFs might not be the feature points in the subsequent IMFs, which describe the overall shape of the data in a global way. To obtain the feature points on point clouds, the feature point is identified to be a real

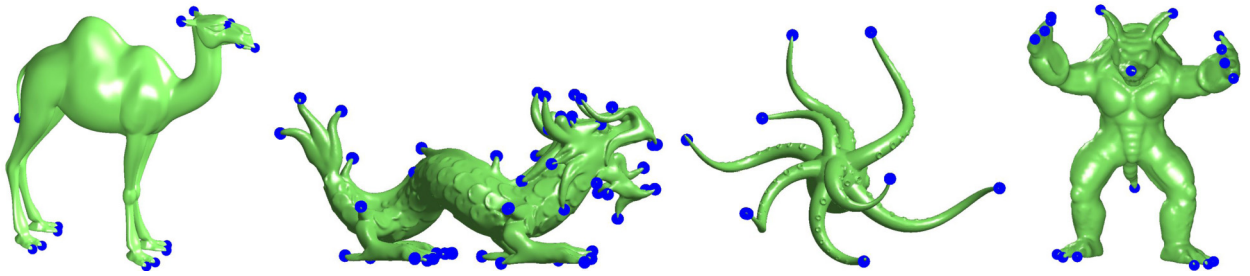


Fig. 9. Feature points detection on different data, including Camel model, Dragon model, Octopus model and Armadillo model.

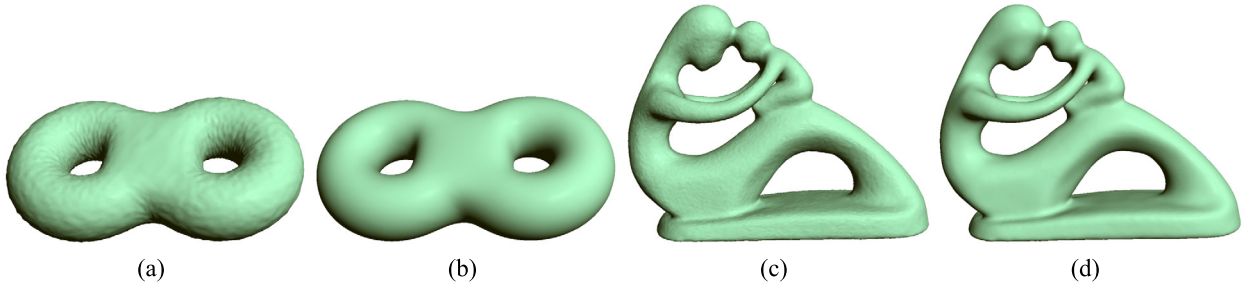


Fig. 10. Denoising results of two simple models. (a) is a noisy torus with two handles. (b) is the denoising result of (a). (c) is the noisy Fertility model. (d) is the denoising result of (c).

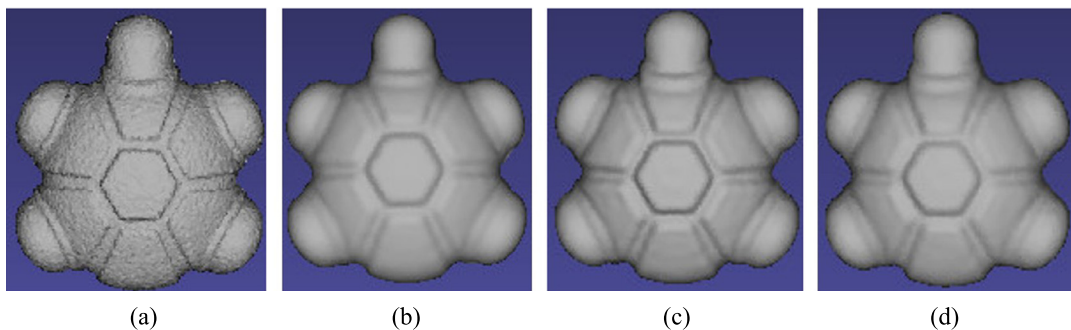


Fig. 11. Denoising results on a noisy toy model. (a) is a noisy toy model. (b) is the denoising result of MLS (Guennebaud and Gross, 2007). (c) is the denoising result of RIMLS (Öztireli et al., 2009). (d) Our result.

feature point if its appearance times in all IMFs exceeds a specific threshold. For enhancing the robustness of feature points detection, more IMFs are needed for achieving feature points detection. In feature points detection, the number of IMFs is set to be 10 as a default and the threshold number of identifying feature points is set to be 8 in our experiments. Fig. 9 shows the feature points extraction on different models within the framework of our proposed EMD-based algorithm.

5.3. Feature-preserving denoising

For noisy models, the noise are contained in the leading IMFs, and will be removed to achieve point clouds denoising. Fig. 10 shows the denoising results of two handle torus and a Fertility model. The two input models are corrupted by 10% Gaussian noise of average distance between neighboring points. Fig. 10(b) is the denoising result reconstructed from the residue, from which we can see that the noise are effectively removed with the overall shape well preserved, as well as the denoising results shown in Fig. 10(d).

Fig. 11 shows the comparing denoising results with moving least squares (MLS) (Guennebaud and Gross, 2007) and robust implicit moving least squares (RIMLS) (Öztireli et al., 2009) on a toy model contaminated with significant noise. Fig. 11(b) is the result of MLS (Guennebaud and Gross, 2007) and Fig. 11(c) is the result of RIMLS (Öztireli et al., 2009), while Fig. 11(d) is our result. From these results, we can see that the significant noise can be removed by the three methods. Since MLS is based on least square approximation, it obtains much smoother result. In contrast, adopting robust local kernel regression and structure measurement, RIMLS and our method generate the denoising result with feature-preserving.

Furthermore, in Fig. 12 the denoising results on two scanned point clouds are shown. Fig. 12(b) is the result obtained by RIMLS, and Fig. 12(c) is the result of our method by abandoning the first two IMFs in signal editing. The noise contained in

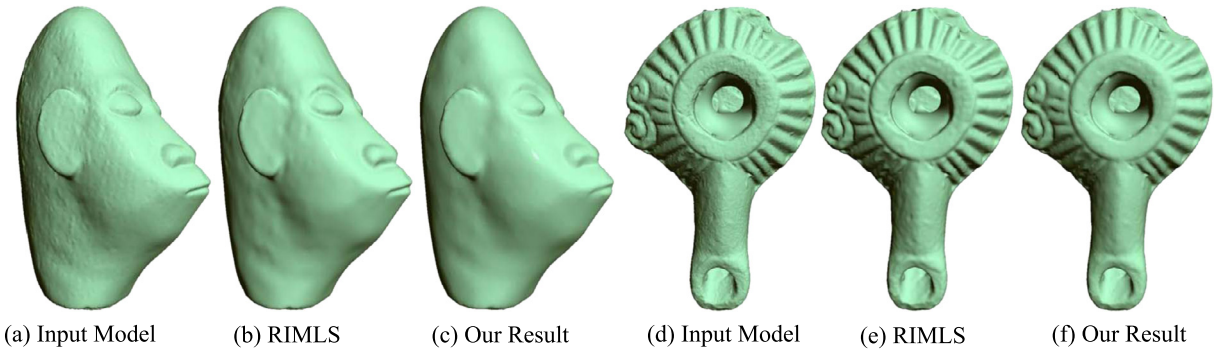


Fig. 12. Denoising results with detail preservation. (a) is a scanned AfroMax model. (b) is the denoising result of RIMLS (Öztireli et al., 2009). (c) Our result. (d) is a scanned archaeological artifact. (e) is the denoising result of RIMLS (Öztireli et al., 2009). (f) Our result.

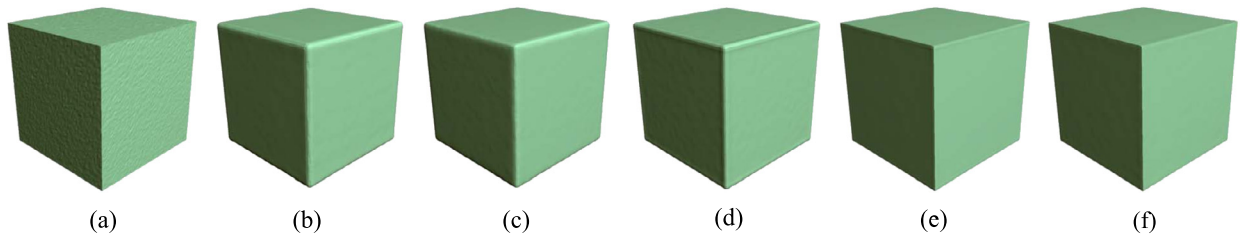


Fig. 13. Comparisons between our method with the previous point clouds denoising algorithms. (a) Input noisy point clouds of cube contaminated with 5% Gaussian noise of average distance between neighboring points. (b) Result of WLOP (Huang et al., 2009). (c) Result of EAR (Huang et al., 2013). (d) Result of MLS (Guennebaud and Gross, 2007). (e) Result of RIMLS (Öztireli et al., 2009). (f) Our result.

the input model are effectively removed while retaining the detail features, which can be observed from the regions of eyes and nose in Fig. 12(b) and Fig. 12(c). Fig. 12(d) is the scanned archaeological artifact with rich details, which is contaminated with noise and geometric details. To obtain the clean model, the proposed mesh-free EMD algorithm is applied to Fig. 12(d). With the assistance of structure measurement in EMD decomposition, the details of the archaeological are well preserved with noise removed (see Fig. 12(f)). Comparing with the results of RIMLS, our method obtains more smoothing results while preserving the geometric details than RIMLS.

Directly applying the extended EMD algorithm on point clouds, the sharp features could not be well preserved. For preserving the sharp features, we further propose a feature-preserving EMD algorithm on point clouds under the assistance of structure measurement. During point cloud denoising, the signal is decomposed using the proposed algorithm and the surface reconstructed from the residue is treated as the final smoothing result. To evaluate the efficiency of our method, we compare the algorithm with the state-of-art algorithms on point clouds denoising, including the weighted locally optimal projection operator (WLOP) (Huang et al., 2009), edge-aware resampling (EAR) (Huang et al., 2013), moving least squares (MLS) algorithm (Guennebaud and Gross, 2007) and RIMLS (Öztireli et al., 2009) in Fig. 13. The results of WLOP in Fig. 13(b) and EAR in Fig. 13(c) are obtained by using the software of Huang et al. (2013) under the guidance provided by the released codes. Fig. 13(d) and (e) are the result of MLS (Guennebaud and Gross, 2007) and RIMLS (Öztireli et al., 2009), which are obtained by utilizing the software of MeshLab. It is observed that all methods can remove noise lying on planar region. However, the WLOP produces a large gap around the sharp edges and results in many crossing artifacts. To overcome this limitation, the upsampling is used to approach the sharp edges in EAR algorithm. The result can be improved to certain extent, but the sharp features still could not be well recovered. In Fig. 13(d), the MLS method performs a smoothing transition around the feature region. In Öztireli et al. (2009), the RIMLS is proposed and the obtained feature-preserving denoising result is shown in Fig. 13(e). Comparing with these algorithms, our method produces a much better result than most previous work and the sharp features are faithfully preserved as well as the result of RIMLS (Öztireli et al., 2009) (see Fig. 13(e) and Fig. 13(f)).

In Fig. 14, Fandisk model is used to further demonstrate the capability of our algorithm to handle noisy data with sharp feature preservation. The Fandisk model is corrupted with 5% Gaussian noise with the average distance between neighboring points. The results shown in Fig. 14(a–g) are obtained by the algorithms of WLOP (Huang et al., 2009), EAR (Huang et al., 2013), MLS (Guennebaud and Gross, 2007), Wang's method (H. Wang et al., 2012), feature-centric EMD (Hu et al., 2014), bilateral filtering (Fleishman et al., 2003) and RIMLS (Öztireli et al., 2009), respectively. From the results shown in the first row, we can see that the sharp features are smoothed together with the noise, although the edge-aware Laplace operator is adopted. Differently, with the sharp feature points extraction, the method of Hu et al. (2014) obtains the sharp feature-preserving result in Fig. 14(e) as well as the results obtained by the bilateral filtering (Fleishman et al., 2003) and RIMLS (Öztireli et al., 2009) in Fig. 14(f) and Fig. 14(g). However, there are still some artifacts occurring on smooth regions

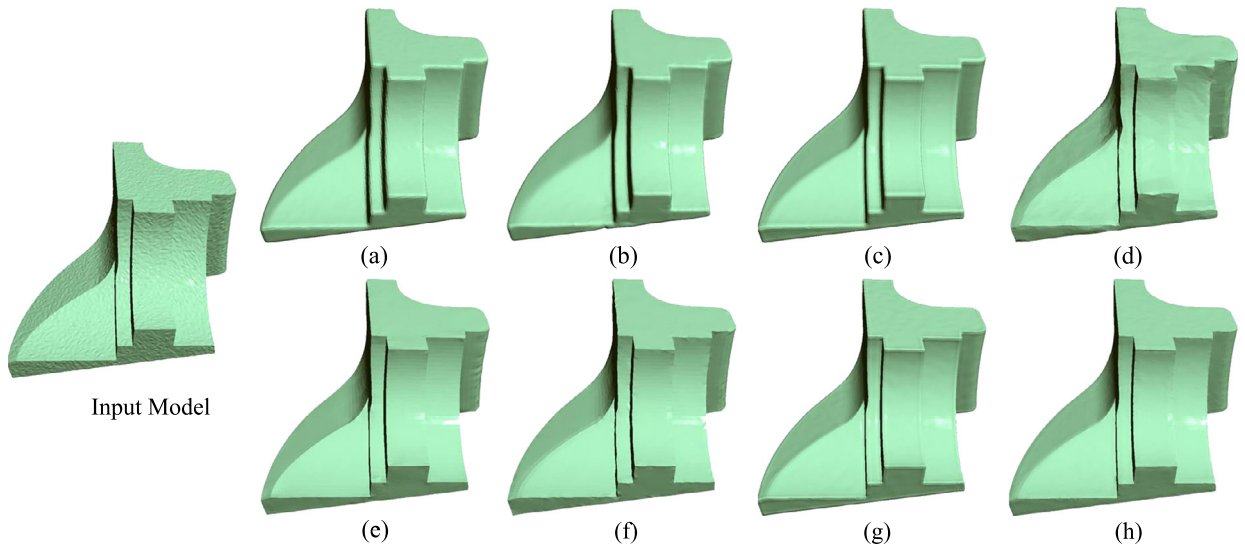


Fig. 14. Feature-preserving result of Fandisk model. Input Fandisk model corrupted by 5% Gaussian noise of average distance between neighboring points. (a) Result of WLOP (Huang et al., 2009). (b) Result of EAR (Huang et al., 2013). (c) Result of MLS (Guennebaud and Gross, 2007). (d) Result of Wang's method (H. Wang et al., 2012). (e) Result of feature-centric EMD (Hu et al., 2014). (f) Result of bilateral filtering (Fleishman et al., 2003). (g) Result of RIMLS (Öztireli et al., 2009). (h) Our result.

Table 1

Run times (in seconds). #P: number of points. #IMF: number of IMFs. #NB: number of neighbors. SM: time of structure measurement computation. LB: time of discrete Laplacian operator construction. EMD: time of signal decomposition. Total: total time of our method.

Figs	#P	#IMF	#NB	SM	LB	EMD	Total
Fig. 1	165954	3	15	36.08	144.11	276.37	470.80
Fig. 6	25038	3	25	3.88	21.76	36.66	64.57
Fig. 9(a)	40240	10	25	6.44	34.78	51.17	111.08
Fig. 9(b)	69827	10	15	12.24	60.45	57.15	151.50
Fig. 9(c)	16944	15	30	2.66	15.78	31.92	65.47
Fig. 9(d)	16805	10	15	2.501	14.42	3.87	36.36
Fig. 10(b)	14142	3	25	2.13	10.59	14.82	30.07
Fig. 10(d)	42514	3	25	6.94	36.89	54.87	103.81
Fig. 12(b)	93047	3	25	17.54	84.15	132.55	247.24
Fig. 12(d)	44445	3	25	7.30	40.17	58.45	111.01
Fig. 12(f)	108744	3	25	20.51	84.15	148.6	279.07
Fig. 13	24578	1	15	3.61	18.65	8.51	37.23
Fig. 14	27827	1	15	5.10	22.42	11.34	42.20

and along the feature lines. With the guidance of structure measurement, our EMD-based algorithm obtains satisfactory result and retains sharp features fully preserved in Fig. 14(h).

5.4. Time performance and parameters

The proposed algorithm is implemented in MATLAB 2013a on a laptop with the Intel Core i7-4790 CPU @ 3.60 GHz with 16.0 GB memory. There are three main stages in our algorithm, point clouds Laplacian operator construction, EMD decomposition, and structure measurement computation in feature-preserving EMD. The time consumption of the entire algorithm depends on the size of input point clouds. It may be noted that, the time performance of three stages is primarily affected by the size of involved neighbors and the number of decomposed IMFs. The more IMFs and the larger number of neighbors are used, the more time will be consumed. Usually, for the point set with the presence of large amount of noise, more neighbors are needed to improve the robustness of the algorithm in applications of smoothing and denoising. On the other hand, smaller size of neighbors should be adopted to capture the small-scale detail features as well as preserve sharp features. Generally speaking, our algorithm is not sensitive to the size of neighbors, and the 15–35 neighbors are typically considered in our experiments.

Apart from the important parameters of neighbor size discussed above, all important parameters are fully discussed in corresponding sections. To obtain satisfactory results, we start the experiments with all parameters in default values, then tune the parameters according to the demands from various applications and the conditions of the input data, such as the

degree of noise and the sharpness of features. The implementation was done in MATLAB without any specific optimization and the used parameters as well as the time of main steps are presented in Table 1.

5.5. Limitation

The proposed EMD-based algorithm represents our first research attempt that aims to extend the EMD on point clouds, even though it has shown significant promise, it still has room for improvement. Suffering from the mode mixing problem of original EMD, the proposed method may not completely distinguish different components in narrow-band signals. That will result in similar scale features appearing in two different IMFs or different scale features mixed in one IMF. This limitation may be ameliorated by restoring to ensemble EMD algorithm and after that we can edit each feature in an independent manner.

6. Conclusion

In this paper, we have developed a novel multi-scale mesh-free EMD algorithm without the need of building explicit connectivity among discrete points. As a result, the salient advantages of EMD techniques on meshed surfaces could be extended directly to unorganized point clouds, hence enhancing the modeling and processing potential of EMD-relevant technologies and broadening their application scopes. The multi-scale representation is achieved by iteratively extracting the detail level from the input signal and retaining the overall shape in residue. For point-based EMD analysis and processing, we further devised a new envelope computational scheme enabled by an anisotropic structure measurement to preserve sharp features with high fidelity. In sharp contrast with available feature-preserving EMD methods for meshed models, our algorithm does not explicitly rely on sharp feature detection, which has made our algorithm more robust to noisy and complex point clouds. A wealth of experiments and comparisons have been provided to demonstrate the utility and efficacy of our multi-scale mesh-free EMD algorithm in various applications of point clouds smoothing and detail enhancing, feature points detection, and feature-preserving denoising.

As for ongoing and near-future research, we will make great efforts to make the algorithm to deal with significant noise, outliers, close-by surface, multi-scale geometric features for point clouds. We are also focusing on the challenging mode-mixing problem of EMD and aiming to achieve a clear separation of features at different scales. In addition, more applications on point clouds (that could be facilitated by the newly-developed EMD algorithm) shall be explored, such as large-scale point clouds editing, point clouds compression, and point clouds completion.

Acknowledgements

The models in this paper are provided by the courtesy of AIM@SHAPE Repository. The model shown in Fig. 12(d) is provided by the Laboratory of Computer Graphics & Multimedia at the Technion. This work is supported in part by National Science Foundation of USA (IIS-1715985, IIS-0949467, IIS-1047715, and IIS-1049448), National Natural Science Foundation of China (No. 61532002, 61672149, 61602341, 11626169); Natural Science Foundation of Tianjin (No. 17JQJNC00600); The open funding project of State Key Laboratory of Virtual Reality Technology and Systems, Beihang University (Grant No. BUAA-VR-16KF-23, BUAA-VR-17KF-04); The technological research foundation of Education Department of Jilin Province (2016097); The Scientific and Technological Development Program Foundation of Jilin Province, China Grant No. 20170520052JH.

References

- Ali, H., Hariharan, M., Yaacob, S., Adom, A.H., 2015. Facial emotion recognition using empirical mode decomposition. *Expert Syst. Appl.* 42 (3), 1261–1277.
- Baghaie, A., Yu, Z., 2006. Image interpolation method based on structure tensor. *J. Comput. Appl.* 26 (7), 1570–1572.
- Belkin, M., Sun, J., Wang, Y., 2009. Constructing Laplace operator from point clouds in R^d . In: *Proceedings of the Twentieth Annual ACM-SIAM Symposium on Discrete Algorithms*, pp. 1031–1040.
- Bernardini, F., Mittleman, J., Rushmeier, H., Silva, C., Taubin, G., 1999. The ball-pivoting algorithm for surface reconstruction. *IEEE Trans. Vis. Comput. Graph.* 5 (4), 349–359.
- Çelebi, A.T., Ertürk, S., 2012. Visual enhancement of underwater images using empirical mode decomposition. *Expert Syst. Appl.* 39 (1), 800–805.
- Di, C., Yang, X., Wang, X., 2014. A four-stage hybrid model for hydrological time series forecasting. *PLoS ONE* 9 (8), e104663.
- Fleishman, S., Drori, I., Cohen-Or, D., 2003. Bilateral mesh denoising. *ACM Trans. Graph.* 22 (3), 950–953.
- Gao, Y., Li, C.-F., Ren, B., Hu, S.-M., 2013. View-dependent multiscale fluid simulation. *IEEE Trans. Vis. Comput. Graph.* 19 (2), 178–188.
- Gemmrich, J.R., Farmer, D.M., 2004. Near-surface turbulence in the presence of breaking waves. *J. Phys. Oceanogr.* 34 (5), 1067–1086.
- Guennebaud, G., Gross, M., 2007. Algebraic point set surfaces. *ACM Trans. Graph.* 26 (3), 23:1–23:9.
- Hammond, D.K., Vandergheynst, P., Gribonval, R., 2011. Wavelets on graphs via spectral graph theory. *Appl. Comput. Harmon. Anal.* 30 (2), 129–150.
- Hu, J., Wang, X., Qin, H., 2014. Improved, feature-centric EMD for 3D surface modeling and processing. *Graph. Models* 76 (5), 340–354.
- Hu, J., Wang, X., Qin, H., 2016. Novel and efficient computation of Hilbert Huang transform on surfaces. *Comput. Aided Geom. Des.* 43, 95–108.
- Huang, N.E., Shen, Z., Long, S.R., Wu, M.C., Shih, H.H., Zheng, Q., Yen, N.-C., Tung, C.C., Liu, H.H., 1998. The empirical mode decomposition and the Hilbert spectrum for nonlinear and non-stationary time series analysis. *Proc. R. Soc. Lond., Ser. A, Math. Phys. Eng. Sci.* 454 (1971), 903–995.
- Huang, N.E., Wu, M.-L.C., Long, S.R., Shen, S.S., Qu, W., Gloersen, P., Fan, K.L., 2003. A confidence limit for the empirical mode decomposition and Hilbert spectral analysis. *Proc. R. Soc. Lond., Ser. A, Math. Phys. Eng. Sci.* 459 (2037), 2317–2345.
- Huang, H., Li, D., Zhang, H., Ascher, U., Cohen-Or, D., 2009. Consolidation of unorganized point clouds for surface reconstruction. *ACM Trans. Graph.* 28 (5), 176–182.
- Huang, H., Wu, S., Gong, M., Cohen-Or, D., Ascher, U., Zhang, H.R., 2013. Edge-aware point set resampling. *ACM Trans. Graph.* 32 (1), 9:1–9:12.

- Kim, H.S., Choi, H.K., Lee, K.H., 2009. Feature detection of triangular meshes based on tensor voting theory. *Comput-Aided Des.* 41 (1), 47–58.
- Kopsinis, Y., McLoughlin, S., 2009. Development of EMD-based denoising methods inspired by wavelet thresholding. *IEEE Trans. Signal Process.* 57 (4), 1351–1362.
- Kramer, H.P., Bruckner, J.B., 1975. Iterations of a non-linear transformation for enhancement of digital images. *Pattern Recognit.* 7 (1–2), 53–58.
- Krinidis, S., Krinidis, M., 2013. Empirical mode decomposition on skeletonization pruning. *Image Vis. Comput.* 31 (8), 533–541.
- Linderhed, A., 2002. 2D empirical mode decompositions in the spirit of image compression. In: *Wavelet and Independent Component Analysis Applications IX*, pp. 1–8.
- Liu, J., Cao, J., Liu, X., Wang, J., Wang, X., Shi, X., 2014. Mendable consistent orientation of point clouds. *Comput-Aided Des.* 55, 26–36.
- Long, S.R., 2005. Applications of HHT in image analysis. In: *Hilbert–Huang Transform and Its Applications*, pp. 289–305.
- Luo, C., 2014. Laplace-Based Spectral Method for Point Cloud Processing. Ph.D. thesis. The Ohio State University.
- Luo, Y., Al-Dossary, S., Marhoon, M., Alfaraj, M., 2003. Generalized Hilbert transform and its applications in geophysics. *Lead. Edge* 22 (3), 198–202.
- Luo, C., Safa, I., Wang, Y., 2009. Approximating gradients for meshes and point clouds via diffusion metric. In: *Proceedings of the Symposium on Geometry Processing. SGP'09*, pp. 1497–1508.
- Mandic, D., Rehman, N., Wu, Z., Huang, N., 2013. Empirical mode decomposition-based time–frequency analysis of multivariate signals: the power of adaptive data analysis. *Signal Process. Mag., IEEE* 30 (6), 74–86.
- Manh, H.T., Yeo, J., Lee, G., 2015. Saliency detection by tensor voting based Gaussian modeling. In: *Proceedings of the 9th International Conference on Ubiquitous Information Management and Communication. IMCOM'15*, pp. 68–75.
- Niang, O., Thioune, A., Gueirea, M.C.E., Del Échelle, E., Lemoine, J., 2012. Partial differential equation-based approach for empirical mode decomposition: application on image analysis. *IEEE Trans. Image Process.* 21 (9), 3991–4001.
- Nunes, J., Bouaoune, Y., Delechelle, E., Niang, O., Bunel, P., 2003. Image analysis by bidimensional empirical mode decomposition. *Image Vis. Comput.* 21 (12), 1019–1026.
- Osher, S., Rudin, L.I., 1990. Feature-oriented image enhancement using shock filters. *SIAM J. Numer. Anal.* 27 (4), 919–940.
- Öztireli, A.C., Guennebaud, G., Gross, M., 2009. Feature preserving point set surfaces based on non-linear kernel regression. *Comput. Graph. Forum* 28 (2), 493–501.
- Park, M.K., Lee, S.J., Lee, K.H., 2012. Multi-scale tensor voting for feature extraction from unstructured point clouds. *Graph. Models* 74 (4), 197–208.
- Prada, M.K., Fabian, 2015. Unconditionally stable shock filters for image and geometry processing. *Comput. Graph. Forum* 34 (5), 201–210.
- Qin, X., Hong, C.X., Zhang, S.Q., Wang, W.H., 2009. EMD based fairing algorithm for mesh surface. In: *CAD/Graphics'09*, pp. 606–609.
- Ren, B., Li, C.-F., Lin, M., Kim, T., Hu, S.-M., 2013. Flow field modulation. *IEEE Trans. Vis. Comput. Graph.* 19 (10), 1708–1719.
- Schneider, E.K., Fennessy, M.J., Kinter III, J.L., 2009. A statistical-dynamical estimate of winter ENSO teleconnections in a future climate. *J. Climate* 22 (24), 6624–6638.
- Subr, K., Soler, C., Durand, F., 2009. Edge-preserving multiscale image decomposition based on local extrema. *ACM Trans. Graph.* 28 (5), 147–155.
- Tsuchie, S., Higashi, M., 2012. Surface mesh denoising with normal tensor framework. *Graph. Models* 74 (4), 130–139.
- Vallet, B., Lévy, B., 2008. Spectral geometry processing with manifold harmonics. *Comput. Graph. Forum* 27 (2), 251–260.
- Wang, X., Cao, J., Liu, X., Li, B., Shi, X., Sun, Y., 2012. Feature detection of triangular meshes via neighbor supporting. *J. Zhejiang Univ. Sci. C* 13 (6), 440–451.
- Wang, H., Su, Z., Cao, J., Wang, Y., Zhang, H., 2012. Empirical mode decomposition on surfaces. *Graph. Models* 74 (4), 173–183.
- Wang, X., Hu, J., Zhang, D., Qin, H., 2015. Efficient EMD and Hilbert spectra computation for 3D geometry processing and analysis via space-filling curve. *Vis. Comput.* 31 (6), 1135–1145.
- Wang, X., Hu, J., Zhang, D., Guo, L., Qin, H., Hao, A., 2017. Multi-scale geometry detail recovery on surfaces via empirical mode decomposition. *Comput. Graph.*, 1–10. <https://doi.org/10.1016/j.cag.2017.07.024>.
- Weickert, J., 2003. Coherence-enhancing shock filters. In: *Pattern Recognition*. In: *Lecture Notes in Computer Science*, vol. 2781. Springer, Berlin, Heidelberg, pp. 1–8.
- Wu, Z., Schneider, E.K., Kirtman, B.P., Sarachik, E.S., Huang, N.E., Tucker, C.J., 2008. The modulated annual cycle: an alternative reference frame for climate anomalies. *Clim. Dyn.* 31 (7–8), 823–841.
- Wu, Z., Huang, N.E., Chen, X., 2009. The multi-dimensional ensemble empirical mode decomposition method. *Adv. Adapt. Data Anal.* 01 (03), 339–372.
- Xie, X., 2014. Illumination preprocessing for face images based on empirical mode decomposition. *Signal Process.* 103, 250–257.
- Xu, Y., Liu, B., Liu, J., Riemenschneider, S., 2006. Two-dimensional empirical mode decomposition by finite elements. *Proc. R. Soc. Lond., Ser. A, Math. Phys. Eng. Sci.* 462, 3081–3096.
- Xu, G., Wang, X.T., Xu, X.G., 2009. Improved bi-dimensional EMD and Hilbert spectrum for the analysis of textures. *Pattern Recognit.* 42 (5), 718–734.
- Xu, K., Zhang, H., Cohen-Or, D., Xiong, Y., 2009. Dynamic harmonic fields for surface processing. *Comput. Graph.* 33 (3), 391–398.
- Zang, Y., Huang, H., Zhang, L., 2014. Efficient structure-aware image smoothing by local extrema on space-filling curve. *IEEE Trans. Vis. Comput. Graph.* 20 (9), 1253–1265.
- Zang, Y., Huang, H., Zhang, L., 2015. Guided adaptive image smoothing via directional anisotropic structure measurement. *IEEE Trans. Vis. Comput. Graph.* 21 (9), 1015–1027.
- Zhang, D., Wang, X., Hu, J., Qin, H., 2017. Interactive modeling of complex geometric details based on empirical mode decomposition for multi-scale 3D shapes. *Comput-Aided Des.* 87, 1–10.